Electronic Supplementary Material (ESI) for Journal of Materials Chemistry C.

Supporting information

High stretchable and anti-freezing silk-based conductive hydrogel for application of self-adhesive and transparent ionotronic skin

*Bohua Zhao, Qianying Chen, Gaohuan Da, Jinrong Yao, Zhengzhong Shao, and Xin Chen**

State Key Laboratory of Molecular Engineering of Polymers, Department of Macromolecular Science, Shanghai Stomatological Hospital, Laboratory of Advanced Materials, Fudan University, 220 Handan Road, Shanghai, 200433, People's Republic of China

*Corresponding author: chenx@fudan.edu.cn

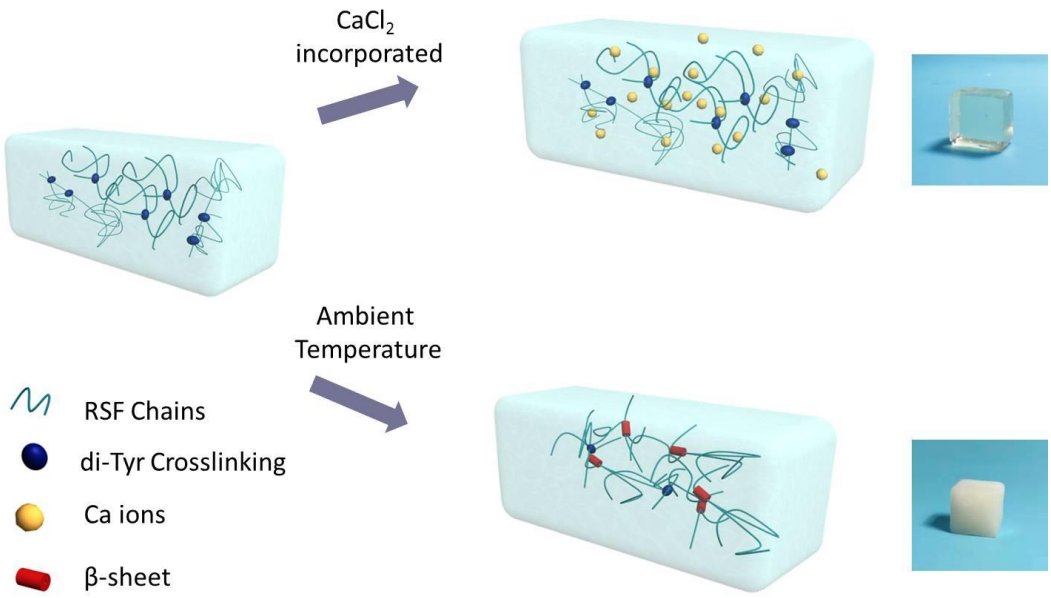

Fig. S1. Schematic illustration of the RSF/HRP hydrogel with or without $CaCl_2$ incorporation.

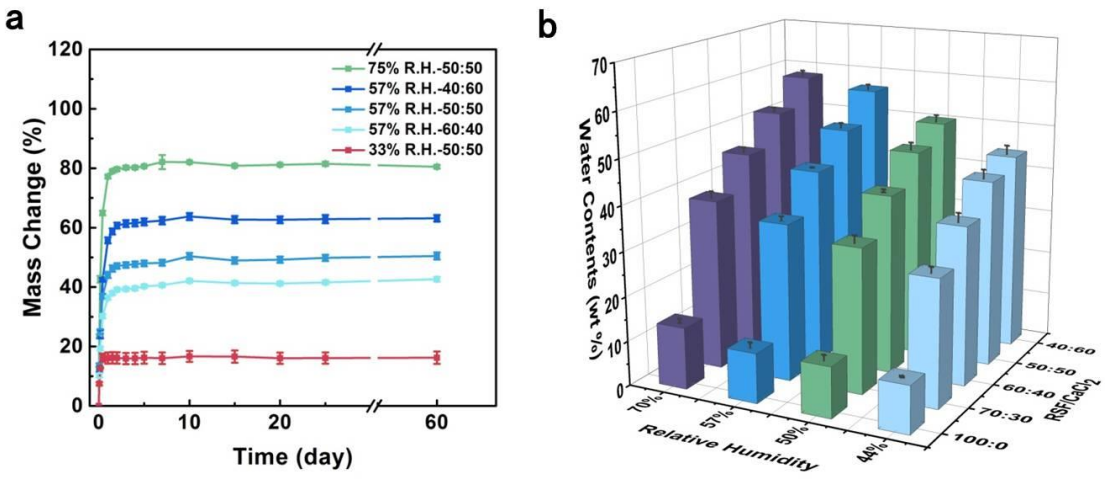

Fig. S2. (a) Mass change of the RSF/$CaCl_2$/HRP hydrogels with different relative humidity. (b) Water content of the RSF/$CaCl_2$/HRP hydrogel at different humidity and RSF/$CaCl_2$ mass ratio (n=3).

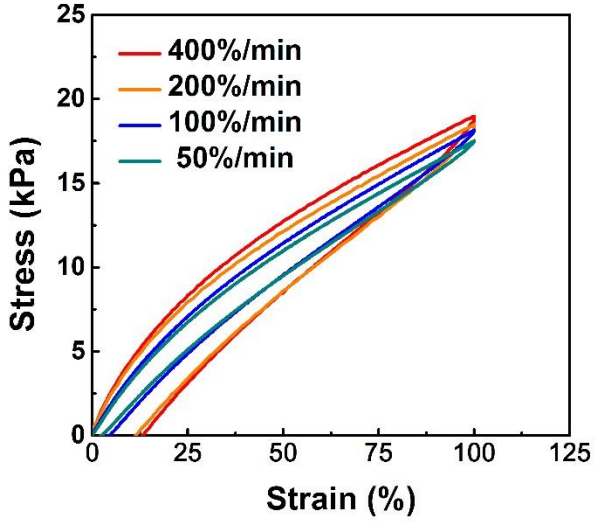

Fig. S3 Loading−unloading curves of the RSF/$CaCl_2$/HRP hydrogels under 100% strain at different loading−unloading rate.

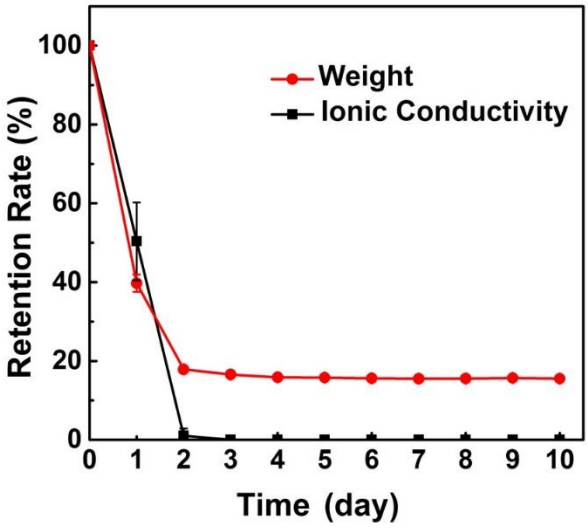

Fig. S4. The stability of the PAAm/SA hydrogel after long-term exposing to ambient air at 50% R.H.

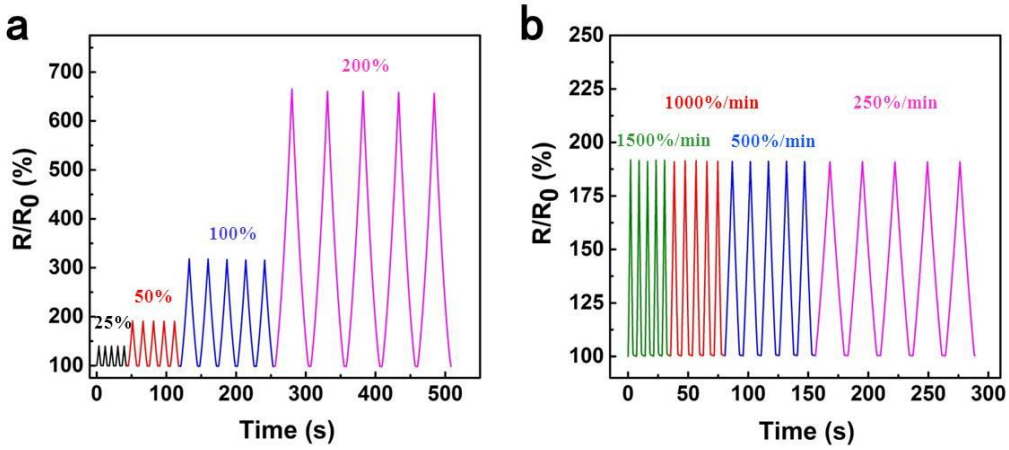

Fig. S5. The variation of the resistance changes of the RSF/$CaCl_2$/HRP hydrogel as a function of the strain and loading–unloading rate. (a) Change of R/R_0 for 5 cycles at different strain of 25%, 50%, 100%, and 200% under a constant loading–unloading rate of 500%/min. (b) Change of R/R_0 for 5 cycles at different loading–unloading rate of 1500%/min, 1000%/min, 500%/min, and 250%/min under a constant strain of 50%.

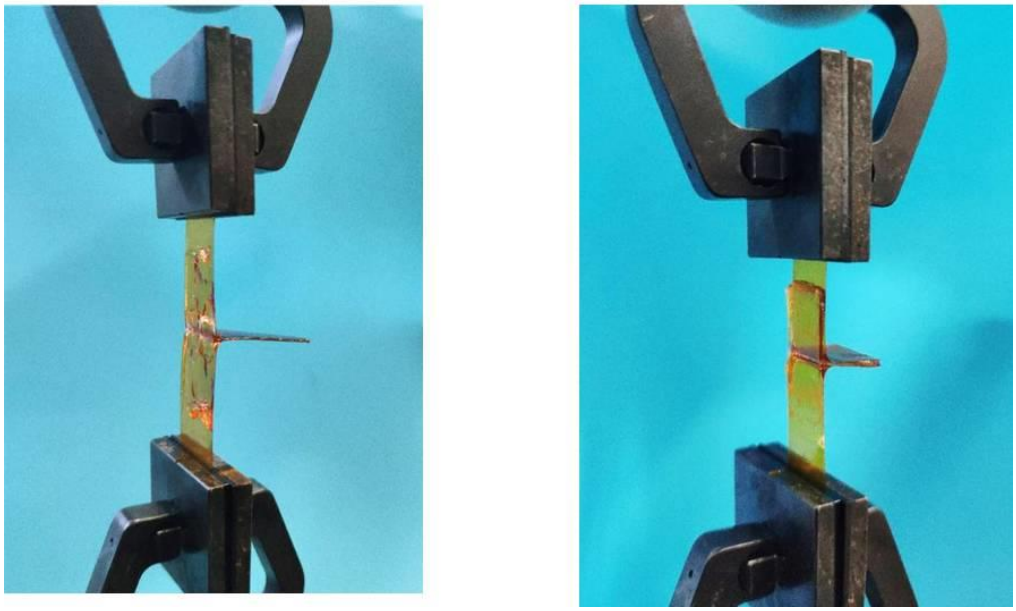

Fig. S6. Optical images of the peeling process. (a) RSF/$CaCl_2$ hydrogel; (b) RSF/$CaCl_2$/HRP hydrogel.

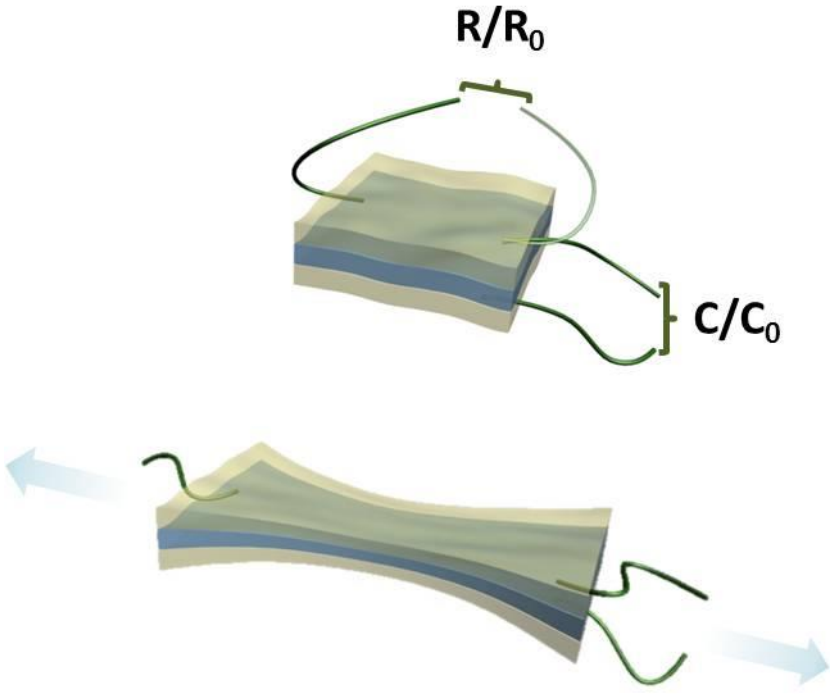

Fig. S7. Schematic structure of the RSF-based dual functional capacitance sensor.

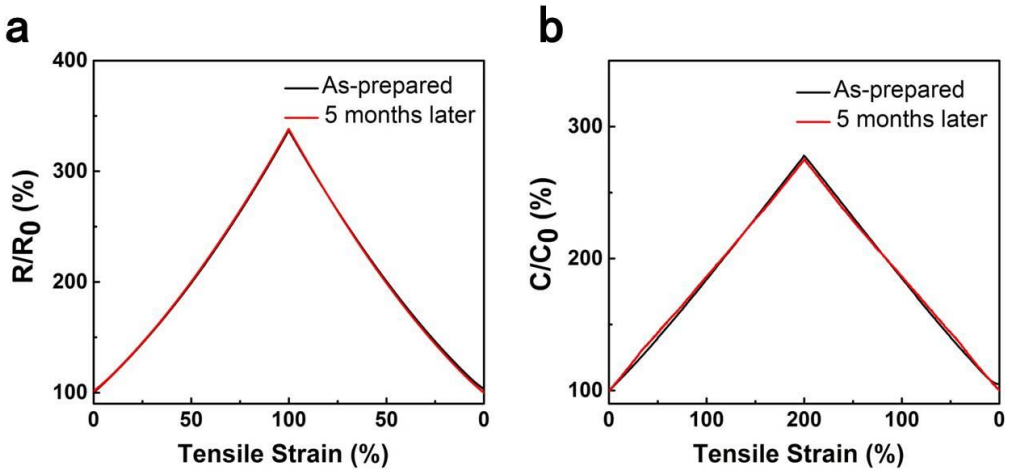

Fig. S8. Stability of the RSF/$CaCl_2$/HRP hydrogel-based sensors. (a) Resistance changes. (b) Capacitance changes.

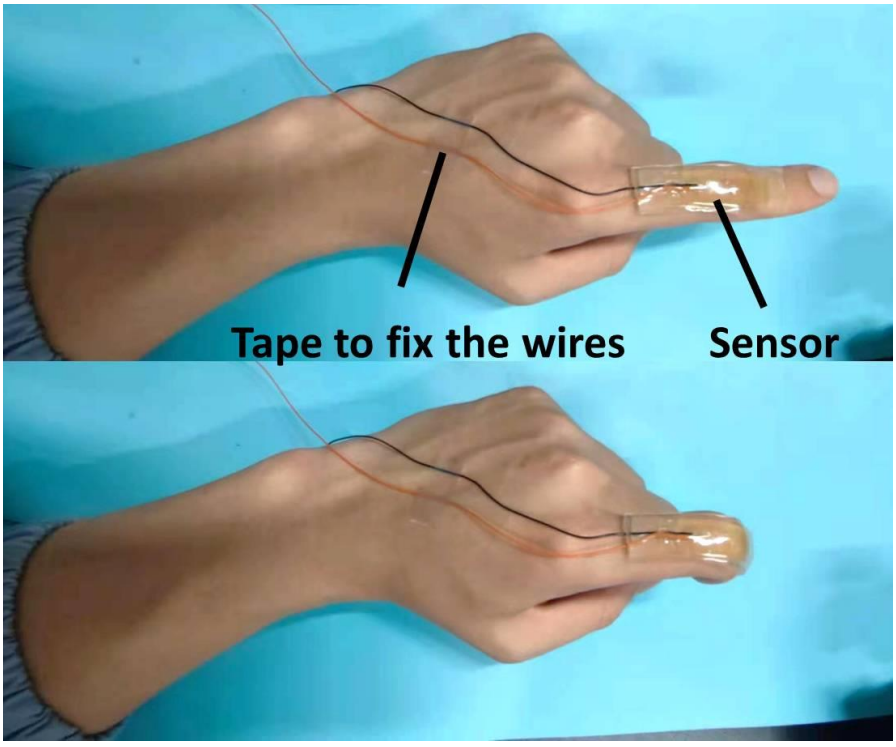

Fig. S9. Demonstration of a RSF hydrogel-based sensor mounting on the volunteer's finger to perform wearable sensing tests.

Table S1. Comparison on the multi-functionality of the hydrogel-based sensors

Materials	Transparency	Self-adhe-siveness	Water Retention	Sensor Type	Working ability below 0 ℃	Ref.
PAA/Chitosan/GO	Opaque	Yes	Yes	Strain	Yes	1
PAM/PDA−talc	Transparent	Yes	No	Strain	No	2
PAA/TA@CNCs/PANI*	Opaque	Yes	No	Strain	No	3
PAA/PVA/Fe(III)	Transparent	No	No	Strain/Pressure/ Temperature	No	4
Ag/TA@CNCs/PVA	Opaque	Yes	No	Strain	No	5
Cellulose/ $BzMe_3NOH$	Transparent	No	No	Pressure/ Temperature	Yes	6
PAM/Carrageenan	Transparent	No	Yes	Temperature	Yes	7
PAA/Fe(III)/PANI NFs	Opaque	Yes	Yes	Strain/ Temperature	No	8
PAAM/SC/CC**	Transparent	Yes	No	Strain	No	9
PAAM/rGO	Opaque	Yes	No	Strain	No	10
RSF/Ca(II)	Transparent	Yes	Yes	Strain/ Temperature	Yes	This Work

*TA@CNCs: tannic acid coated cellulose nanocrystals.

**SC: sodium caseinate; CC: carboxymethyl chitosan.

References:

1. S. Xia, S. Song, Y. Li and G. Gao, *J. Mater. Chem. C*, 2019, **7**, 11303-11314.
2. X. Jing, H. Mi, Y. Lin, E. Enriquez, X. Peng and L. Turng, *ACS Appl. Mater. Interfaces*, 2018, **10**, 20897-20909.
3. C. Shao, L. Meng, C. Cui and J. Yang, *J. Mater. Chem. C*, 2019, **7**, 15208-15218.
4. S. Shin, W. Lee, S. Kim, M. Lee, J. M. Koo, S. Y. Hwang, D. X. Oh and J. Park, *Chem. Eng. J.*, 2019, **371**, 452-460.
5. F. Lin, Z. Wang, Y. Shen, L. Tang, P. Zhang, Y. Wang, Y. Chen, B. Huang and B. Lu, *J. Mater. Chem. A*, 2019, **7**, 26442-26455.
6. Y. Wang, L. Zhang and A. Lu, *ACS Appl. Mater. Interfaces*, 2019, **11**, 41710-41716.
7. J. Wu, Z. Wu, Y. Wei, H. Ding, W. Huang, X. Gui, W. Shi, Y. Shen, K. Tao and X. Xie, *ACS Appl. Mater. Interfaces*, 2020, **12**, 19069-19079.
8. G. Ge, Y. Lu, X. Qu, W. Zhao, Y. Ren, W. Wang, Q. Wang, W. Huang and X. Dong, *ACS Nano*, 2020, **14**, 218-228.
9. G. Wang, Q. Zhang, Q. Wang, L. Zhou and G. Gao, *ACS Appl. Mater. Interfaces*, 2021.
10. X. Zheng, Y. Gao, X. Ren and G. Gao, *J. Mater. Chem. C*, 2021, **9**, 3343-3351.